DD

CLRC

Technical Report
RAL-TR-1999-022

A Gas Microstrip Detector for X-Ray Imaging with Readout of the Anode by Resistive Divide

J E Bateman J F Connolly A B Lodge R Stephenson R Mutikainen I Suni and J Morse

8th April 1999

COUNCIL FOR THE CENTRAL LABORATORY OF THE RESEARCH COUNCILS

Enquiries about copyright, reproduction and requests for
additional copies of this report should be addressed to:

The Central Laboratory of the Research Councils
Library and Information Services
Rutherford Appleton Laboratory
Chilton
Didcot
Oxfordshire
OX11 0QX
Tel: 01235 445384 Fax: 01235 446403
E-mail library@rl.ac.uk

ISSN 1358-6254

RAL-TR-1999-022

A GAS MICROSTRIP DETECTOR FOR X-RAY IMAGING WITH READOUT OF THE ANODE BY RESISTIVE DIVIDE

J E Bateman, J F Connolly, A B Lodge and R Stephenson,
Rutherford Appleton Laboratory, Chilton, Didcot, OX11 0QX, UK,

R Mutikainen[+] and I Suni,
VTT Electronics, P O Box 1101, 02044VTT, Espoo, Finland

J Morse,
ESRF, B P 220, 38043 Grenoble, France

Abstract

The results are presented of a development programme aimed at the validation of the key concepts and technologies for the construction of a 2-d x-ray detector based on gas microstrip detector technology using resistive divide along the anode to achieve the second dimension. A prototype detector and its associated electronic readout system have been developed which demonstrate the capability of a spatial resolution (standard deviation) of approximately 1/1000 of the working aperture combined with readout rates of up to 400kHz per anode.

+

[+] Now at VTI Hamlin Oy, P O Box 27, FIN-01621 Vantaa, Finland

1. INTRODUCTION

Following its introduction by Oed [1] and its successful development as a high resolution (<0.1mm) high rate tracking detector in particle physics [2] it was natural to consider the potential of the gas microstrip detector (GMSD) for x-ray imaging applications in the context of sychrotron radiation sources. Sub-millimeter readout resolution is readily attained in one dimension with the GMSD by means of the intrinsic digitisation of the anode-cathode strip pattern (typically a few hundred microns in period) and detectors of this type for SR applications are well under way [3,4]. When, however, 2-dimensional readout is desired the traditional forms of readout applied to gas counters (such as delay lines) are rendered impracticable by the relatively low gas gain (<5000) which can be achieved reliably in the GMSD. Noting that it is possible to achieve specific resistance values of >10kΩ/cm during the fabrication of the 10μm wide anode strips (which is typical of the values used in the readout of wire proportional counters) we decided to investigate the possibility of achieving fast resistive divide on an anode-by-anode basis with sufficient spatial resolution and speed to be attractive for SR applications.

A preliminary investigation of the fabrication and electronic problems associated with this form of readout indicated that the potential existed for an x-ray imager with a specification which would be very attractive in the context of SR applications. In order to investigate the technical problems associated with the development of such a detector a Collaboration Contract (no. CL 0016) was issued by the ESRF Council. The work described in this report was carried out under this contact.

Within the limited funding, effort was concentrated on generating a series of prototype devices which aimed to solve the key technical problems: on the one hand in the GMSD itself and on the other in the dedicated, front-end (analogue) electronics required for fast readout. As a result of this program we were eventually able to demonstrate spatial resolution of around 0.1mm RMS (σ) for 5.9keV x-rays over an active anode length of 120mm delivered by electronics capable of functioning at rates up to 400kHz per anode.

2. GENERAL DESIGN PRINCIPLES

The (conflicting) requirements of the design are for maximum spatial resolution and maximum rate capability. How these requirements interact can be seen from the following considerations.

2.1 Spatial resolution

Figure 1 shows the basic principles of the resistive divide readout. The ends of the resistive anode strip are connected to low noise charge preamplifiers (mounted locally to the detector) which in turn feed the shaping amplifiers which preceed the analogue computer which calculates the position parameter. It follows from the simple sum used to calculate the position of an event from the charge signals at each end of the anode strip: $X = (Q_L - Q_R)/(Q_L + Q_R)$, where Q_L and Q_R are the left and right hand pulses, that the RMS spatial resolution obtainable is simply

$$\sigma_X = L_a \sigma_Q / (Q_L + Q_R) \quad \{1\}$$

where L_a is the length of the anode strip and σ_Q is the RMS charge noise in the Q_{sum} (= Q_L+Q_R) signal.

In the practical case (when low noise charge preamplifiers are used) σ_Q is dominated by the differential noise signal generated by the resistance of the anode strip which may be evaluated by the usual parallel resistor noise formula:

$$\sigma_Q^2 = 2SkT\tau/R \qquad \{2\}$$

where S is the weighting factor appropriate to a given pulse shaping network (S=1.85 for CR-RC shaping), k is Bolzmann's Constant, T is the absolute temperature, τ is the shaping time constant (assumed symmetric), R is the resistor value and σ_Q is the RMS noise charge in coulombs.

In seeking to minimise σ_Q, formula {2} immediately points up a conflict between minimising τ and maximising R. The minimum value of τ is set by the need to capture a significant fraction of the charge associated with the x-ray event. In the GMSD positive ion collection times are such that about 200ns integration time is quite adequate in general. However, another factor slowing the delivery of charge to the preamplifiers is the nature of the anode strip structure which (electrically) looks like an RC transmission line. Thus R must be kept low enough to deliver the charge within the shaping time and cannot be made arbitrarily high. If R_a and C_a are the anode resistance and capacitance to earth then from the properties of delay lines it is obvious that τ must be proportional to R_aC_a and that σ_Q will minimise for $\tau \approx R_aC_a$ with a minimum value which is proportional to $1/C_a$. (This reflects the general property of counter readouts that the ultimate resolution is inversely proportional to the stray capacity of the collection electrode.)

Fortunately the stray capacity of the anode strips of a GMSD is low - around 0.2pF/cm and in the case of the present design (L_a=13.8cm, R_a=130kΩ, C_a=2.4pF) $R_aC_a \approx$300ns which matches well to the ion collection time and comfortably permits counting rates of several hundred kHz. For practical reasons τ was set at 500ns in our design.

Evaluating σ_Q with S=1.85, τ=0.5μs and R=1.3×10^5 Ω gives σ_Q=1491 electrons. With an 8keV x-ray giving 300 electrons and a gas gain in the GMSD of 5000, the total charge signal, $Q_{sum}=1.5\times10^6$ electrons. Thus from equation {1} we would expect an RMS spatial resolution $\sigma_x = 120*1491/1.5\times10^6 = 0.14$mm. This is close to the desired specification for the detector.

2.2 Rate Capability

The ultimate rate limit in a gas detector is set by space charge effects. In the standard design with strips spaced at 0.3mm the practical rate limit was found to be at around 250kHz/mm^2 at a gain of 1000 [5]. At a gas gain of 5000 this scales back to 50kHz/mm^2 or 16.7kHz/mm of anode length. This is a local rate limit which could lead to a maximum readout channel rate of 2MHz. It is therefore a major design requirement to derive the position signal $X = (Q_L - Q_R)/(Q_L + Q_R)$ in as short a time as possible (<1µs) and with the maximum stability against rate-induced errors.

It immediately became obvious that in order to meet this requirement it was essential to use bipolar (delay line) pulse shaping. In this type of shaping delay line clipped images of the preamplifier pulse are combined to give a bipolar pulse [6]. Analysis shows that this network results in a rate-induced base line shift proportional to $(\tau_{dl}/\tau_{pa})^2$ where τ_{dl} is the time constant of the shaping delay line and τ_{pa} is the decay time constant of the charge preamplifier. Typically $(\tau_{dl}/\tau_{pa})^2 \approx 1/10000$, so that the rate-induced errors in X remain tolerable even at very high rates. Unipolar pulse shaping generates a base-line shift proportional to τ_{dl}/τ_{pa} and so is much inferior in this respect. However, there is a significant penalty in the noise performance relative to (say) RC shaping. Experience shows that in the case of bipolar shaping the shape factor S (equation {2}) is approximately twice the value expected for CR-RC shaping.

It was decided that the calculation of X within the desired period of 1µs was best achieved by means of an analogue computer. With this approach the position pulse height is automatically available at the peak of the anode pulse, i.e. at about 500ns after the start of the event. The remaining 500ns of the bipolar pulse could then be used for the digitisation and storage of the position information giving a complete cycle time per event of close to 1µs.

3. GMSD FABRICATION

In order to simplify the problem of connection to the detector strips in the prototype devices (normally wire bonding is used) the simplified mask design shown in figure 2 was made. The anode width and the anode-cathode gap are standard at 10µm and 90µm respectively. However the cathode strips are made 9.79mm wide so that the period of the pattern is 10mm and there is ample room for large pads at the ends of the strips to which simple pressure connections can be made.

The development proceeded in three stages with the pattern produced in chrome (nominally 0.5µm thick) on 100mm square Tempax glass plates, 100mm square S8900 glass plates and finally on 178mm x 178mm S8900 glass plates. In order to adjust its resistivity the chrome was doped with oxygen during the reactive sputtering deposition process by introducing oxygen into the sputtering ambient. Standard photolithography and wet chemical etching were utilised to to form the anode tracks with a total resisistance in the region of 130kΩ in all cases. The results presented in this report are all taken from the large plate which had a total anode length of 138mm with an active length of 126mm. The seven anodes on the plate tested showed a mean resistance of 130.5kΩ with a standard deviation of 5.15kΩ. All the plate fabrication was carried out at VTT Electronics.

The plates were mounted in a sealed gas enclosure with a thin foil drift electrode spaced 9mm above the glass plate. A thin foil window in the enclosure gave access to the ^{55}Fe x-rays used for the tests. Each section of the counter could be powered independently. A gas mixture of argon with 25% isobutane was used routinely.

4. ELECTRONIC DESIGN AND PRODUCTION

As explained in the introduction the electronic design effort was concentrated on the problem of delivering an analogue position signal from one anode ready for digitisation, the data handling problem being left till a later stage. The analogue electronic processing system falls naturally into four parts (figure 1):

- The low-noise charge sensitive preamplifiers
- The bipolar pulse shapers
- The analogue computer
- The timing circuits
- The analogue output circuits

4.1 The charge preamplifiers

These circuits were developed for applications of GMSDs in Particle Physics [7] in a compact format of sixteen channels on a small card which can be stacked in such a way as to service the connection density of 30 channels/cm of counter. This matches the density proposed for a full-scale 2-dimensional x-ray detector. The feedback elements can be selected to suit any particular application. In the present case they consist of a 3.3pF capacitor and a 33MΩ resistor to give charge to voltage conversion with a pulse decay time of 100μs. The amplifier rise time is about 10ns.

4.2 The bipolar pulse shapers

The bipolar pulse shaper is implemented by means of a 1μs tapped DIL delay line serviced by three fast operational amplifiers (EL2020 and EL2232) which combine the clipped and delayed images of the input pulse. Only one trim is required to assure the balance of the output pulse.

4.3 The analogue computer

The analogue computer consists of a pair of operational amplifiers to generate the SUM and DIFFERENCE signals (AD811) and the 10MHz, 4-Quadrant Divider - AD734. The latter has a dynamic range of ±10V combined with high slew rate, low noise and low distortion. For example: it can settle to 0.1% of the correct output in 200ns at full power. As will be shown below, this device contributes negligibly to the position resolution of the system. Particular care is taken with the baseline of the denominator (DIFFERENCE) signal to prevent large deadtime arising from the Divider sitting at full scale when no denominator is present.

The most important set-up for the analogue computer is the provision of a means to reduce any DC offset in the DIFFERENCE channel to a minimum since any such offset leads to a pulse-height-dependent slewing error in *X*.

4.4 The timing circuits

These consist of a simple discriminator, operating on the SUM pulse, which with a timing monostable generates the trigger for the sample and hold module which is following the output of the analogue computer and a gate for the linear gate which puts the *X* signal out onto the analogue ouput port. Provision is made for the mutual inhibition of adjacent strips of the GMSD which happen (occasionally) to trigger together. A DATA READY pulse is provided for the trigger of the digital part of the data aquisition system.

4.5 The output circuits

The output X signal pulse is generated by the trigger pulse locking the sample and hold circuit (AD781) which is tracking the output of the Divider and opening a linear gate (DG419) to put a 0.5μs pulse (0-10V) on the analogue output port.

As indicated in figure 1, the final "production" version of the prototype electronic system was packaged in a double width NIM module which houses four channels of readout with the various housekeeping functions (deadtime etc.) necessary for a complete system.

5. SYSTEM PERFORMANCE

The detector was operated with an argon + 25% isobutane gas mixture with typically, a drift electrode potential (V_D) of -2000V and a cathode potential (V_C) of between -650V and -700V. These potentials gave gas gains in the region of 4000 to 8000. Figure 3 shows the pulses (^{55}Fe x-rays) observed at the SUM pulse test point on a CRT (the bipolar part of the pulse is not transmitted to the test output). The clear full-energy and escape peaks are identifiable and appear clearly when the pulses are delivered to a pulse height analyser (PHA) - figure 4. The FWHM of the full-energy peak is approximately 20%. The tail of low pulse heights is due to the partial collection of events on the fringe of the sensitive volume of the drift region (see discussion below).

5.1 Imaging Performance

The imaging performance of the detector system was measured by means of a very highly collimated ^{55}Fe x-ray source projected onto the detector through a slit of 0.15mm width. A monte-carlo model of the collimator predicts that the standard deviation of the beam projection on the detector is 99μm. Figure 5 shows the histogram of the X pulses recorded in the PHA from this set-up. The counter is moved 10mm under the beam to give the spatial calibration (15.4 channels/mm) between the two observed x-ray peaks. The electronic test pulser (delivered equally into each preamplifier) shows the contribution to the spatial resolution from the white (resistor) noise in the system when the pulse height is matched to the SUM pulse height shown by the x-rays.

As figure 5 shows, at this pulse height level ($2.4\mathrm{x}10^6$ electrons) the white noise makes only a partial contribution to the observed spatial resolution of $\sigma_x = 0.166$mm. The contributions (RMS) to the spatial broadening are:

- collimator projection = 0.099mm
- white noise = 0.091mm
- photoelectron range = 0.0424mm
- diffusion spread of the drift electrons = 0.016mm

Adding the above in quadrature gives $\sigma_x = 0.142$mm which comes close to the observed value. The remaining contribution is probably a result of the finite range of SUM pulse height used. This will be discussed further below.

Leaving aside the collimator contribution, the spatial resolution is dictated principally by the signal to noise ratio (SNR) in the electronic circuits even at the largest SUM pulse heights and as the SUM pulse height decreases this becomes even more true (equation {1}). The performance of the system is therefore best studied using the injected electronic pulses which simulate an event at centre field. Figure 6 shows a plot of σ_x as a function of the equivalent x-ray pulse height in the SUM signal. As expected from equation {1} the spatial resolution depends approximately on 1/SUM. The small constant term added represents the noise of the Divider and the output analogue circuitry. While not entirely negligible, its contribution at a level of 0.048mm is not significant. The front-end (i.e. resistor) noise is given by b/L_a in figure 6, i.e. $3.02\mathrm{x}10^5/138 = 2188.4$ electrons.

Since the x-ray pulse-height spectrum in not in general monochromatic (see figure 4) it is important that the analogue computer output (*X*) does not slew with pulse height. The lower curve in figure 6 shows that with careful setting up, the slewing contribution for a dynamic range of 2:1 can be kept well below the white noise contribution over the useful working range of pulse height (i.e. $>10^6$ electrons). If the setting up of the analogue computer is not correct (i.e. a DC offset is left in the DIFFERENCE channel) then the finite spead of the pulse height distribution produces an asymmetric distortion of the position data (tailing towards low values of *X*) which can be very significant at lower pulse heights.

The excellent linearity of the position parameter (*X*) and the uniformity of σ_x as a function of position along the length of an anode are shown in figure 7. The larger value of σ_x (relative to figure 5) is simply a result of the use of a larger collimator to make the time scale of the measurements practicable.

The uniformity of sensitivity of the counter was measured by placing the ^{55}Fe source 600mm above the counter to give an approximately uniform flood. Figure 8 shows the PHA spectrum when the position signals are histogrammed in this configuration.

A test of the ultimate spatial resolution attainable from the detector was set up using the finest collimator possible and adjusting the threshold so that only the full-energy peak triggered the readout. The counter is at maximum gain delivering $2.5\mathrm{x}10^6$ electrons in the full energy peak. Figure 9 shows the point spread function observed on the PHA under these conditions. As can be observed, the peak fits best to a sum of gaussians (rather than a single one) which, no doubt, reflects the convolution of the white noise response with the non-gaussian pulse height spectrum. The narrower gaussian fits 60% of the events in a distribution with σ_1 =0.101mm and 40% in one with σ_2=0.257mm. Since the predicted collimator contribution is 0.99mm it is impossible to say exactly what the core response may be beyond that it is better than 0.1mm.

5.2 Rate performance

As discussed above the rate performance has two distinct components, a local limitation (set by space charge effects in the counter) and a global limit (set by the readout electronics). The local limit could not be explored with the ^{55}Fe source and the predicted limit of about 16kHz/mm for one of the prototype strips must await confirmation by means of tests on an x-ray set or SR source. The global limit can be explored since the ^{55}Fe source can raise the global rate to around 1Mhz.

The rate performance of the electronic systems were explored by inserting identical test pulses into the two preamplifiers of a readout channel at a fixed rate (1kHz) and simultaneously gating the analogue output of the system (*X*) into a PHA while the random rate of x-ray events in the counter was varied by moving the ^{55}Fe source closer to the counter window. The PHA was thus only required to count at 1kHz while the analogue electronic system was processing the full random rate. The test pulses represented a mid-field simulated beam, the width and position of which could be monitored as the x-ray flux was varied. The measured rate of the test pulses (relative to 1kHz) gave the throughput efficiency of the system.

Figure 10 shows the results obtained from a typical electronic channel as the random x-ray rate (measured at the Data Ready output) was varied between 0kHz and 400kHz. The spatial resolution deteriorates slowly from its zero frequency value but has only doubled at 200kHz and rate-dependent slewing is satisfactorily absent throughout the range tested.

The usual deadtime formula indicates that the slope of the graph of 1/(counting efficiency) versus output rate should be a measure of the system deadtime. As the fit in figure 10 shows this evaluates at 0.00114ms (i.e. 1.14μs), close to the design aim of 1μs.

5.3 Y-sensitivity

While not designed primarily for use as as a simple 1-dimensional counter, the prototype electrode design does provide a useful additional property for 1-d operation, namely electronic control of the sensitive width at right angles to the anode direction (Y). Due to the large cathode area, increasing the drift field tends to take the electron clouds from x-ray events to the cathode rather than the anode. Thus, as figure 11 shows, by varying the drift potential from -1000V to -2000V one can change the Y active profile from an approximate gaussian of 2.5mm FWHM to one of 1mm FWHM.

The shape of the Y sensitivity can also be controlled by varying the depth of the conversion region and by the insertion of simple auxiliary drift electrodes.

6. DISCUSSION

The results reported above may be discussed under the following headings:

6.1 Spatial resolution vs global rate

Figure 9 shows that the desired spatial resolution (standard deviation) of just over 0.1mm (i.e. approximately 1000σ in an active length of 120mm) is achieved with 5.9keV x-rays and a gas gain of 8000 from the GMSD. Deterioration of this figure with rate is inevitable because of the base-line noise generated by previous events. Figure 10 shows that the rate induced broadening contribution fits very well to a quadratic function of the random rate. The linear term can be attributed to the random offset caused by the residual tails of the bipolar pulses and the quadratic as being due to the pile-up of one pulse on another. The magnitude of the effect is such that at 100kHz the rate-induced broadening (standard deviation) is 0.027mm, at 200kHz:0.096mm, at 300kHz:0.204mm and at 400kHz:0.354mm.

For the very best spatial resolution to be preserved, single channel readout rates should be maintained below 200kHz. However, in many applications some degradation of the spatial resolution is acceptable and rates of up to 400kHz per channel may be accepted.

6.2 Spatial resolution vs x-ray energy

As equation {1} shows, the spatial resolution attainable in the detector depends only on the system noise and the SUM pulse height. Since the former is essentially fixed, the resolution depends inversely on the product of the gas gain and the x-ray energy. Since the counter gas gain in use is at the top end of what is practicable for stable operation, this detector system is not well adapted for use with very soft x-rays. Taking the useful threshold of x-ray energy as around 3keV, the imaging performance will improve with x-ray energy until the photoelectron range becomes significant (≈8keV for argon at 1 bar and ≈12keV in xenon at 1 bar). There would seem to be no reason why moderately hyperbaric operation should not be possible for increased efficiency at higher x-ray energies.

6.3 Spatial resolution vs local rate

Increasing the counter gas gain gives (the other factors being negligible) a pro-rata improvement in the spatial resolution of the counter. Since the space charge effects are also proportional to the gas gain one will see a corresponding decline in the local rate capability of the detector. Thus if the highest resolution is required for narrow peaks, the x-ray rate must be monitored to avoid saturation.

6.4 Spatial resolution and multi-strip operation

The aim of the 2-d detector design is to exploit the small transverse (Y) dimensions possible with gas microstrip design. The inevitable electron diffusion in the drift space confuses this situation somewhat. In a 10mm drift in our standard filling gas an electron cloud will spread out to approximately a gaussian of σ=0.22mm. Thus in general, the charge from an x-ray will be distributed between two adjacent strips which leads to a poor pulse height spectrum in any one strip. However, a monte-carlo simulation of the diffusion process shows that if a threshold of 50% of the x-ray energy is set in each channel then very few events are lost and only one channel generally triggers. This gives the discriminator a dynamic range of 2:1 and makes the point spread function a convolution of gaussians with σs spread over a range of 2:1. This leads to a non-gaussian curve which preserves some of the highest resolving power of the biggest pulses while exhibiting tails induced by the smaller pulses. On average one can expect the effective σ_x to be ≈50% greater than the values reported above when the full pulse height is available.

In single channel operation the spatial resolution benefits from the good pulse height spectrum (as in figure 4) but the local rate capability is put under pressure because of the summing of all the Y distribution at the same point on the anode. The electronic Y collimation discussed in section 5.3 above could be useful in controlling the local rate on the anode.

7. CONCLUSIONS

The results presented above show that the design goals of the ESRF Collaboration Contract have been essentially met by the GMSD and electronic hardware developed for it. Spatial resolution for ^{55}Fe x-rays of close to 0.1mm (standard deviation) has been achieved and the electronic system has been shown to operate stably at rates up to 400kHz.

Clearly, much work remains to be done to elaborate the prototypes described above into a multichannel system capable of acquiring data at global rates of several hundred MHz. However, the plate production process used for the prototype was very little different from standard operations and the main problem still outstanding would be that of handling the more complex bonding scheme required for access to both ends of the anode.

The electronic readout has been already developed to fairly high level of production engineering, though a different packaging system would clearly be required for hundreds of channels. The components used are standard and the setting up procedures are simple and speedy. All the handshake and interfacing facilities have been included to permit smooth implementation of a digital data capture back-end system.

In the absence of funding for a full 2-dimensional implementation, it is interesting to consider the application of the prototype systems to 1-d x-ray readout. The performance reported above offers attractions for experiments for which 1-d detectors have been traditionally used. All the hardware exists for such applications and the digital data capture system required for a single channel is not expensive.

REFERENCES

1. A Oed, Nucl Instr & Meth A263 (1988) 351-359

2. F Angelini, R Bellazzini, A Brez, M M Massai, G Spandre, M R Torquati, R Bouclier, J Gauden, and F Sauli, IEEE Trans Nucl Sci NS-37 (2) (1990) 112

3. W Bras, G E Derbyshire, A J Ryan, G R Mant, A Felton, R Lewis, C Hall, and N Greaves, Nucl Instr & Meth A326 (1993) 587

4. J E Bateman, J F Connolly, G E Derbyshire, A S Marsh, R Stephenson, R C Farrow, W I Helsby, B R Dobson, R Mutikainen and I Suni, Rutherford Appleton Laboratory report no. RAL-TR-1998-073

5. J E Bateman and J F Connolly, Rutherford Appleton Laboratory report no. RAL-93-096

6. P W Nicholson, in: Nuclear Electronics (Wiley, London, 1974) 103-108

7. J E Bateman, J F Connolly, R Stephenson, M Edwards, J C Thompson, Nucl Instr & Meth A348 (1994) 372-377

FIGURE CAPTIONS

Figure 1 Schematic representation of a single channel of resistive anode readout with the associated processing electronics. The double-width NIM module houses four sets of processing electronics with the necessary handshake functions.

Figure 2 A plot of the mask pattern used to fabricate the large prototype GMSD plates. Dimensions are in mm.

Figure 3 A CRT trace of the SUM pulses generated on a single anode by ^{55}Fe x-rays incident at the centre of the anode. Only the leading half of the bipolar pulse is extracted to the test point. (V_D=-1800V, V_C=-650V, charge calibration of full energy peak = 2.7x10^6 electrons)

Figure 4 PHA spectrum of SUM pulse heights obtained in a flood of a single anode by a ^{55}Fe x-ray source (V_D=-2000V, V_C=-684V).

Figure 5 PHA spectrum of the position output pulses (*X*) when a single anode is illuminated by a slit beam of approximately 0.1mm width (σ). (V_D=-2000V, V_C=-672V.) The beam is moved 10mm for spatial calibration. The test pulser is set to the same amplitude as the x-ray full energy peak.

Figure 6 The observed spatial resolution (σ) and position slewing of the position output pulse (*X*) as a function of the amplitude of the test pulse (SUM).

Figure 7 The linearity of the position pulse (X) and the uniformity of the position resolution (σx) as a function of position along the length of an anode. (V_D=-2000V, V_C=-680V, ^{55}Fe x-rays with σ=0.18mm beam width)

Figure 8 The PHA position pulse spectrum obtained with a flood source of ^{55}Fe x-rays. (V_D=-2000V, V_C=-663V)

Figure 9 Position pulse PHA spectrum of the σ=0.1mm wide ^{55}Fe x-ray beam taken with the discriminator set to catch only the full energy peak. Full energy peak charge calibration = 2.5×10^6 electrons.

Figure 10 The performance of the processing electronics as measured by the test pulser in the presence of high rates of x-ray pulses.

Figure 11 The sensitivity of an anode to a slit (0.18mm) beam scanned tranversely to the anode strip direction (Y). The drift potentials (V_D) are successively -1000V, -1500V, -2000V while V_C is held at -702V.

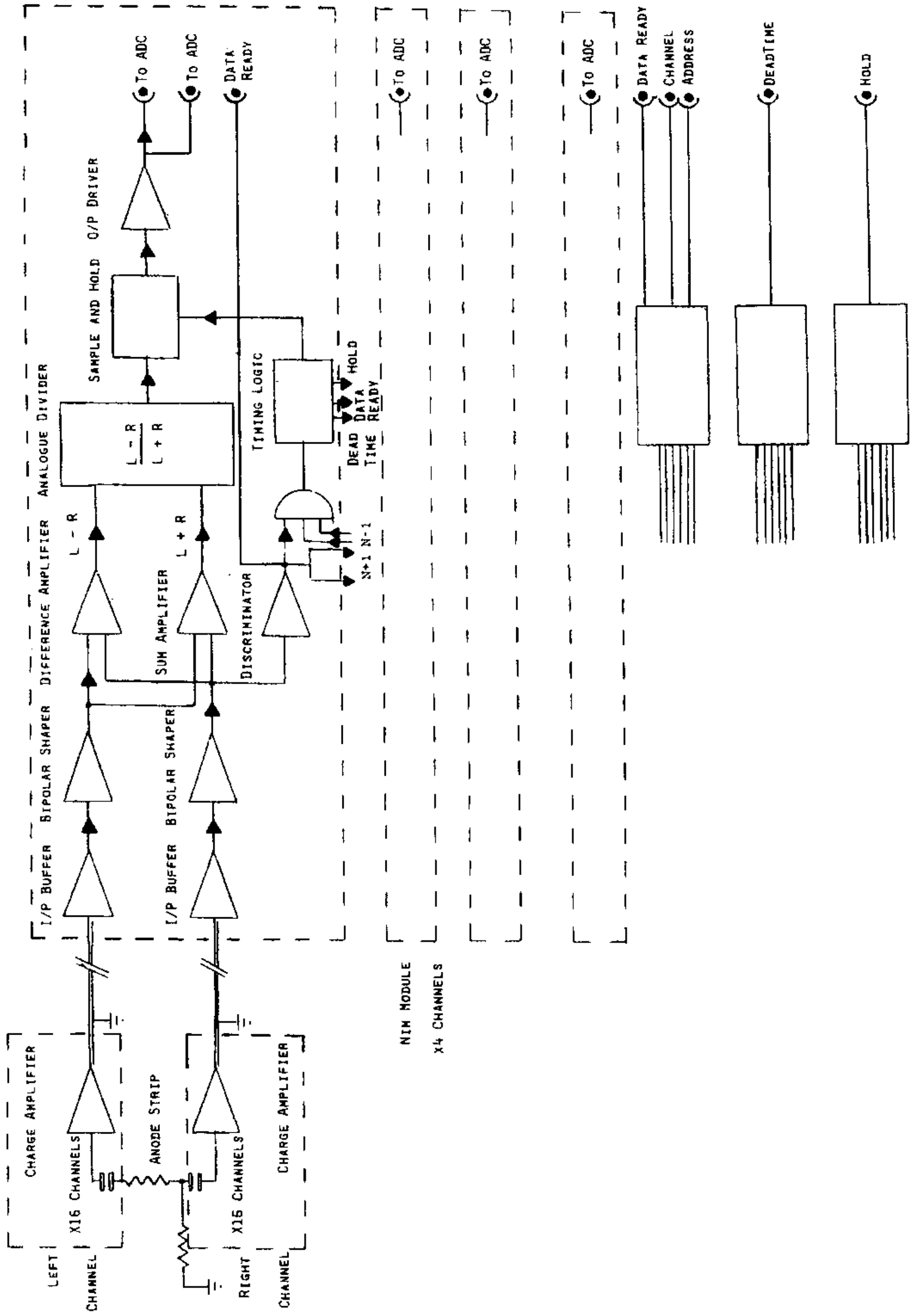
Left Channel
Charge Amplifier
X16 Channels
Anode Strip
Right Channel
Charge Amplifier
X16 Channels
I/P Buffer
Bipolar Shaper
Difference Amplifier
Analogue Divider
Sample and Hold
O/P Driver
To ADC
To ADC
Data Ready
I/P Buffer
Bipolar Shaper
Sum Amplifier
Discriminator
Timing Logic
L - R
L + R
L - R / L + R
Hold
Data Ready
Dead Time
N+1
N-1
To ADC
To ADC
To ADC
NIM Module
x4 Channels
Data Ready
Channel Address
DeadTime
Hold

FIGURE 1

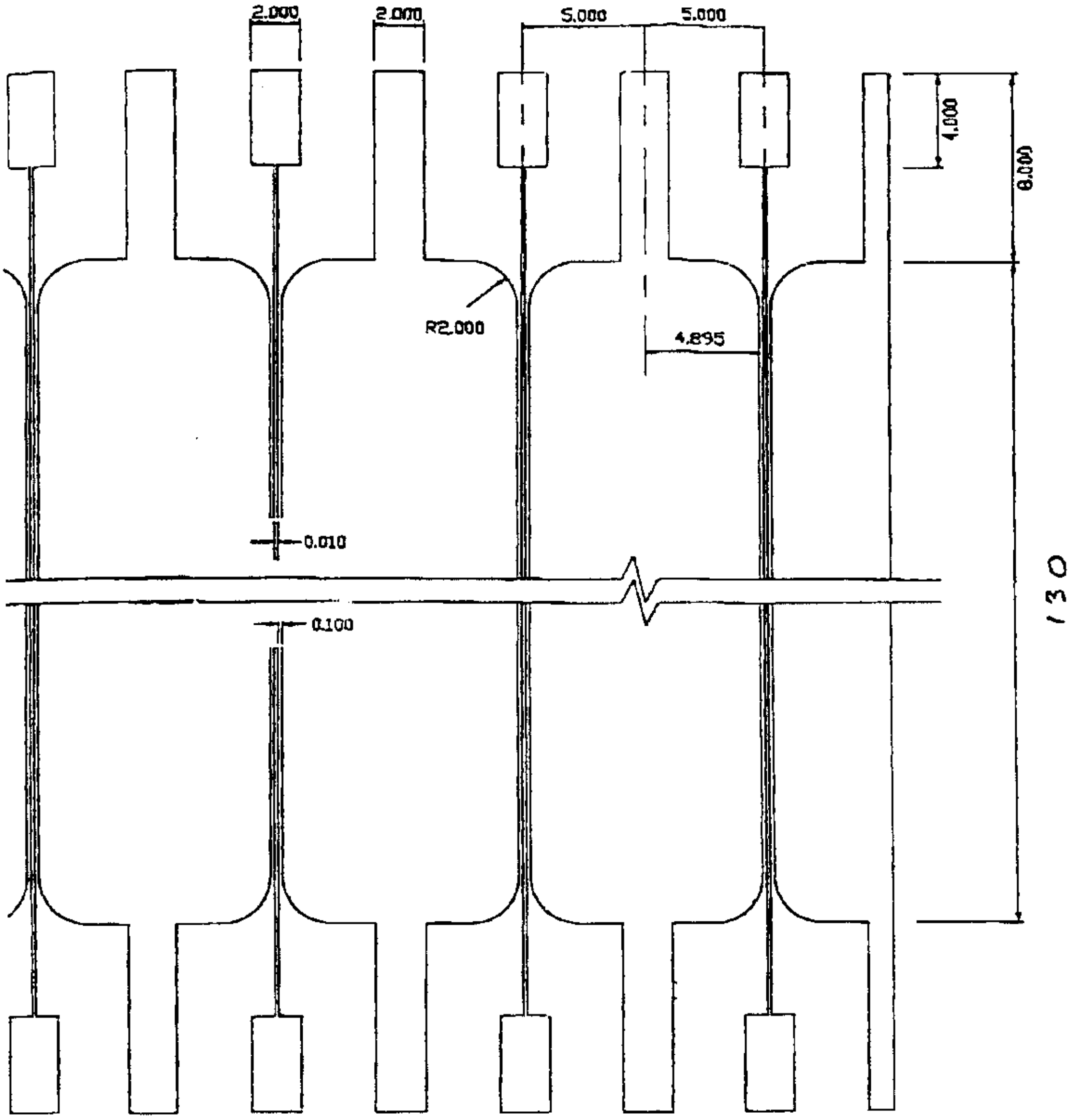

FIGURE 2

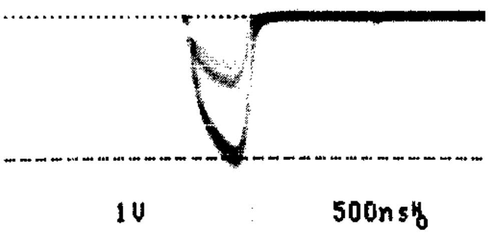

FIGURE 3

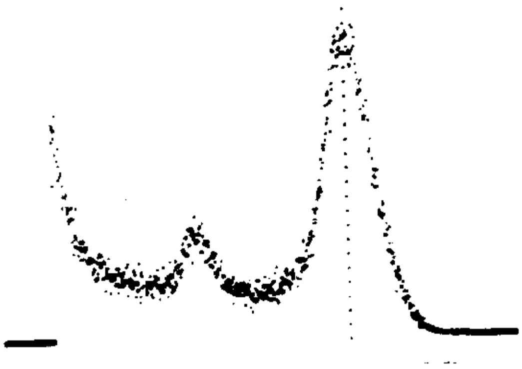

FIGURE 4

FIGURE 5

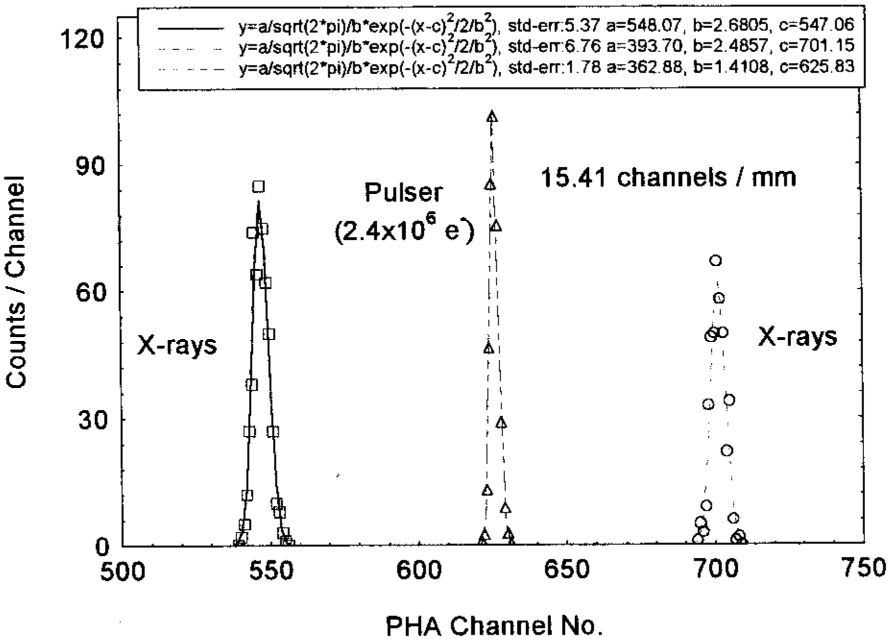

FIGURE 6

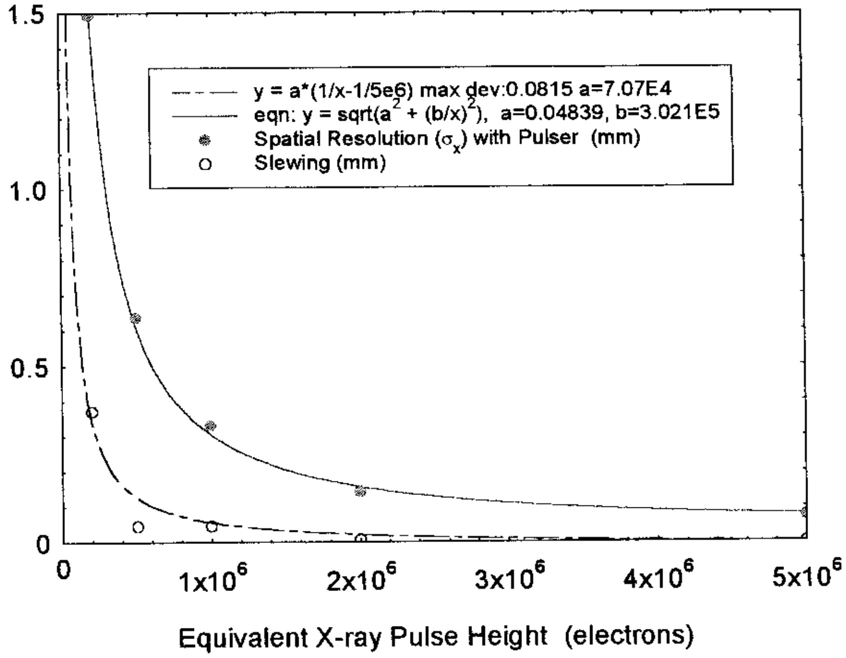

FIGURE 7

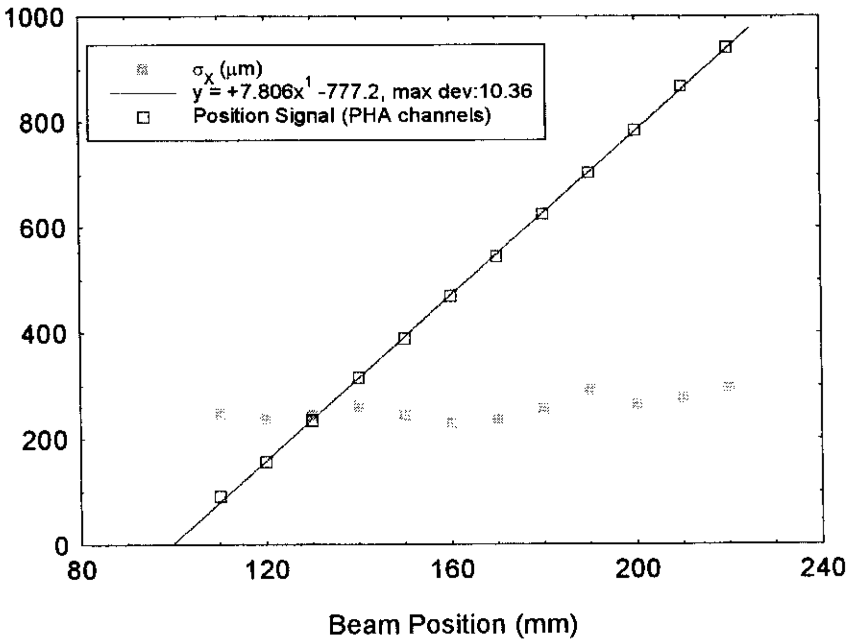

FIGURE 8

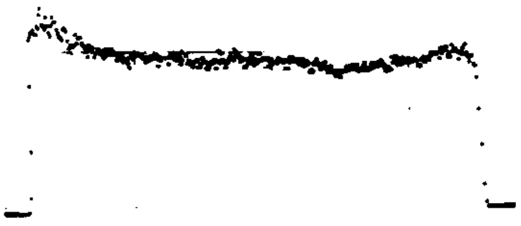

FIGURE 9

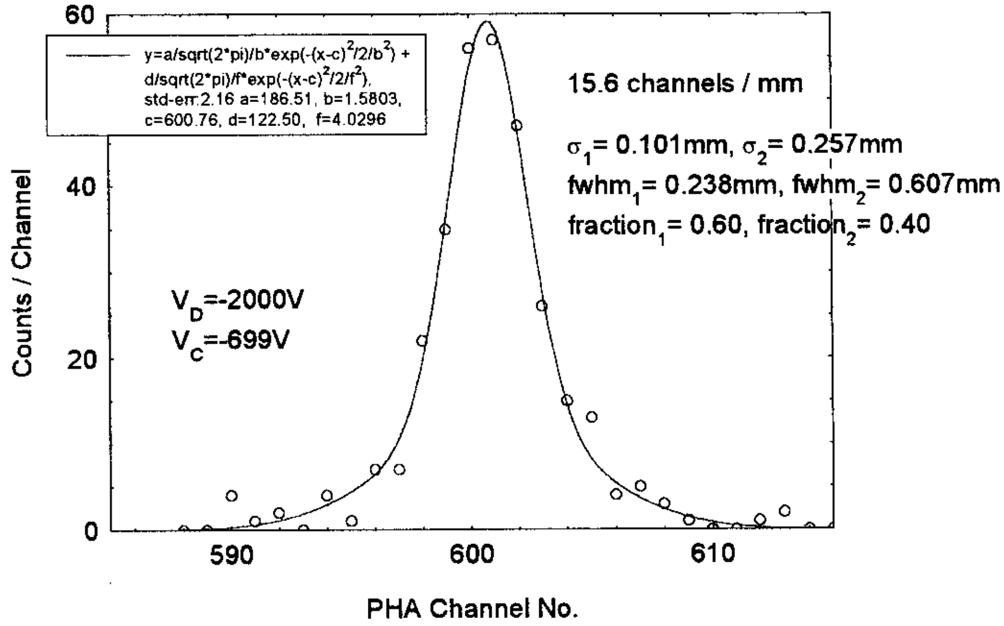

FIGURE 10

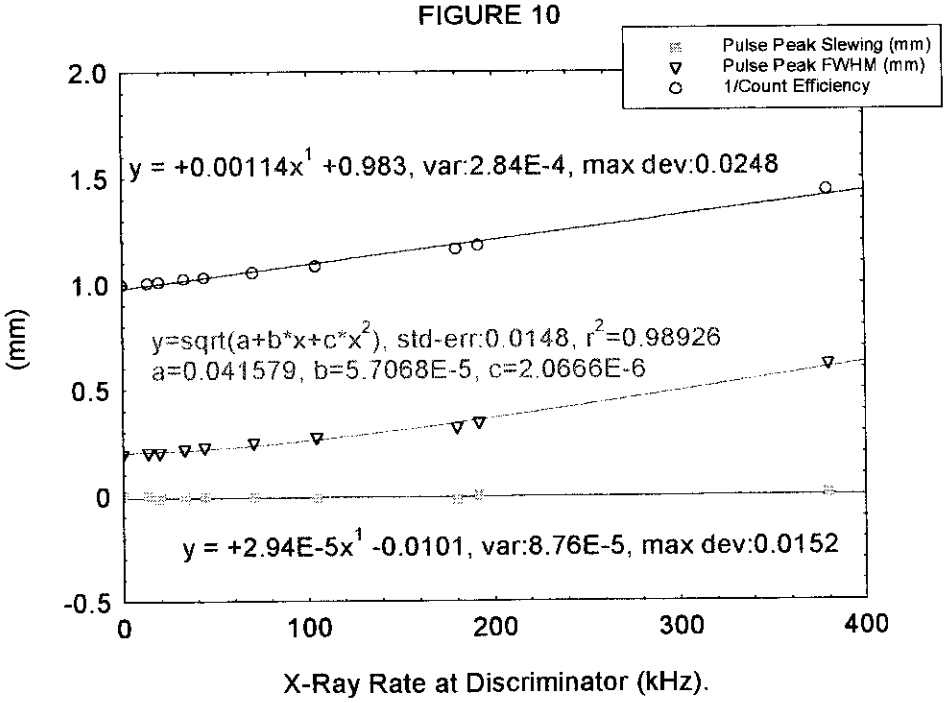

FIGURE 11

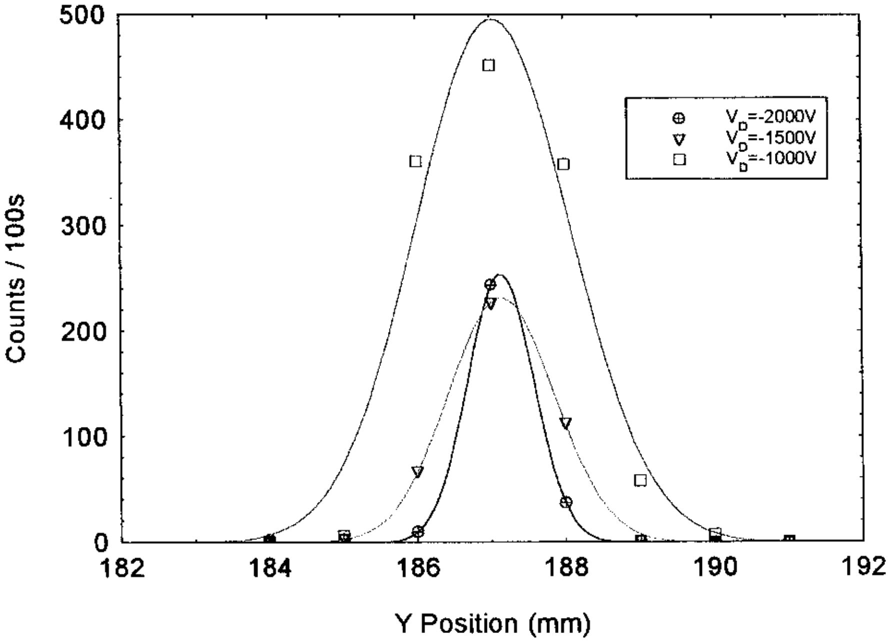
500
400
300
200
100
0
Counts / 100s
182
184
186
188
190
192
Y Position (mm)
⊕ V_D=-2000V
▽ V_D=-1500V
□ V_D=-1000V